Diffusion Brazing Metallurgy of IN718/Ni-Cr-Si-B-Fe/IN718

Correlation between solute redistribution, microstructure development, and shear strength properties of diffusion brazed cast IN718 is studied

BY M. POURANVARI, A. EKRAMI, AND A. H. KOKABI

ABSTRACT

This paper investigates the effect of microstructure development on mechanical properties of diffusion brazed IN718 nickel-based superalloy using a Ni-Cr-Si-B-Fe filler metal. The phase transformations during diffusion brazing of IN718/Ni-Cr-Si-B-Fe/IN718, which dictate the microstructure of the bonds are governed by diffusion-induced isothermal solidification, cooling-induced athermal solidification, and diffusion-induced solid-state precipitation. It was found that when partial isothermal solidification occurs at the bonding temperature, the residual liquid is transformed into eutectic-type microconstituents. Considering solute redistribution and segregation behavior of the melting point depressant elements (Si and B), the solidification behavior of the liquid phase is discussed. Moreover, extensive Cr-Mo-Nb-rich boride precipitates were formed in the substrate region due to solid-state boron diffusion into the base metal during the bonding process. Increasing bonding time resulted in progress of isothermal solidification and an intermetallic-free joint centerline was obtained after 40 min holding at 1050°C. Mechanical properties of the joints are described using hardness profile and room-temperature shear testing. It was found that the presence of a continuous network of intermetallic-containing eutectic-type microconstituents in the joint centerline acts as the preferential failure source and leads to a semi-cleavage brittle fracture with low load-bearing capacity. Completion of isothermal solidification, which guarantees the formation of a ductile single-phase solid-solution joint centerline, improves the shear strength of the bond up to 75% of the base metal.

Introduction

The superalloy Inconel® 718 (IN718) is one of the most frequently used materials in critical aero-engine and space applications for high-temperature, creep-resistant applications such as in nuclear power plants and the petrochemical industry (Ref. 1). The strength of IN718 is governed by both solid-solution and precipitation-hardening mechanisms. While both ordered face-centered cubic (FCC) γ'-$Ni_3(Al,Ti)$ and metastable ordered body-centered tetragonal (BCT) γ''-Ni_3Nb precipitates are formed during the aging cycle of the alloy, the predominant contribution to precipitation hardening is provided by the latter (Ref. 2).

M. POURANVARI (mpouranvari@yahoo.com) *is with Materials and Metallurgical Engineering Department, Dezful Branch, Islamic Azad University, Dezful, Iran. A. EKRAMI and A. H. KOKABI are with Department of Materials Science and Engineering, Sharif University of Technology, Tehran, Iran.*

Fusion welding and brazing are two primary repairing/joining techniques for superalloys that have been commonly applied in industry (Ref. 3). Conventionally, high-temperature brazing, using nickel-based filler alloys, are extensively used as a standard repair/regeneration technique for superalloy components (Refs. 4, 5). In order to lower the liquidus temperature of nickel-based superalloys and increase the fluidity of the braze, melting point depressants (MPD) and modifiers such as phosphorus, silicon, and boron are added to the braze alloy. However, these elements are incorporated into intermetallic phases such as borides, silicides, and phosphides during nonequilibrium eutectic-type solidification of the liquid phase during cooling stage of the brazing process (Refs. 6, 7). The presence of intermetallic phases in the brazed joint's centerline is known to detrimentally affect the performance of the joint in several ways:

- Reducing the mechanical properties (Refs. 8–11).
- Lowering the remelting temperature and service temperature of the brazed component due to segregation of melting point depressants into low melting point eutectic (Ref. 12).
- Reducing the corrosion and oxidation resistance of the brazed component (Ref. 12).

While the sluggish kinetics of γ'' precipitation make IN718 welds free of strain age cracking (Ref. 13), the welding of IN718 suffers from some problems, including

1. Microfissuring and liquation cracking in the HAZ (Refs. 14, 1).
2. The segregation of Nb during nonequilibrium solidification of the fusion zone and the consequent formation of the Nb-rich Laves phase: It has been shown that the formation of the Laves phase 1) depletes principal alloying elements required for precipitation hardening from the matrix, 2) acts as preferential sites for easy crack initiation and propagation due to its inherent brittleness, and 3) deteriorates the mechanical properties, especially tensile ductility, fracture toughness, fatigue, and creep rupture properties (Refs. 1, 15, 16).

Transient liquid phase bonding or diffusion brazing is considered as preferred repairing/joining process for nickel-based superalloys (Refs. 3, 12, 17–22), which is a hybrid process that combines the beneficial features of liquid phase bonding and solid-state bonding. In general, it is considered that there are three distinct stages during diffusion brazing: base metal dissolution, isothermal solidification, and solid-state homogenization (Ref. 18). Combining isothermal solidification with a subsequent solid-state homogenization treatment offers the possibility of producing bonds that are almost chemically iden-

KEYWORDS

Diffusion Brazing
Isothermal Solidification
Inconel 718 (In718)
Solute Redistribution
Mechanical Properties

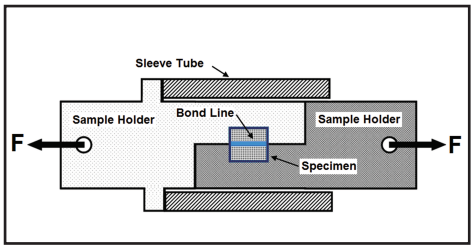

Fig. 1 — Schematic of shear test fixture (Ref. 10).

tical to the base material and have no discernable microstructural discontinuity at the bond line (Refs. 12, 18).

Despite extensive application of IN718 in various industries, there are few published works (Ref. 9) on diffusion brazing of this superalloy. There are some modeling efforts regarding isothermal solidification time of wrought IN718 alloy (Ref. 9); however, there is limited information regarding microstructure development and mechanical properties during diffusion brazing of this superalloy. Therefore, this paper aims at investigating the metallurgy of diffusion brazing of cast IN718 nickel-based superalloy using Ni-Cr-Fe-B-Si filler metal.

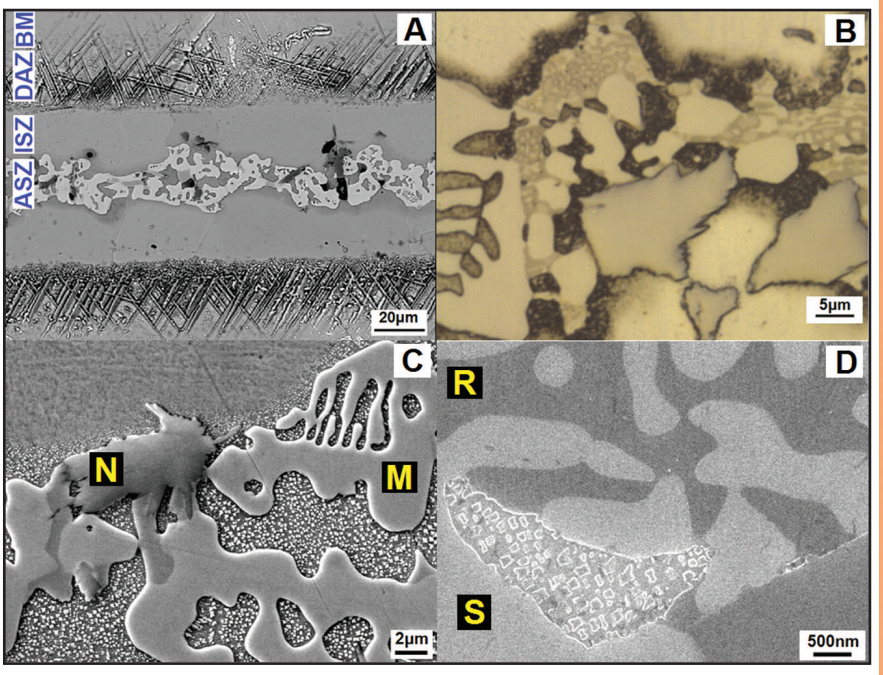

Fig. 2 — Microstructure of diffusion brazed IN718/Ni-Cr-Si-B-Fe/IN718 after partial isothermal solidification. A — Backscattered electron micrograph of joint cross section indicating four distinct zones: ASZ, ISZ, DAZ, and BM; B — optical micrograph showing detailed view of ASZ microconstituents; C — SEM micrograph of Ni-rich boride and Cr-rich boride (M and N indicate Ni-rich boride and Cr-rich boride, respectively); D — SEM micrograph showing detailed view of Ni-Si-B ternary eutectic (R and S indicate Ni-rich silicide and Ni-rich boride, respectively).

Experimental Procedure

A cast IN718 nickel-based superalloy was used as the base metal in this investigation. The chemical composition of the base metal is Ni-20Fe-18Cr-5Nb-3Mo-0.2Si (wt-%). A 50-μm-thick amorphous Ni-based filler metal of BNi-2 (Ni-7Cr-4.5Si-3.2B-3Fe) was used as the interlayer for diffusion brazing. In this filler metal, both B and Si play important roles, being very effective melting-point depressant elements that facilitate wetting.

Coupons sized at 10 × 5 × 5 mm were sectioned from the base metal using an electrodischarge machine. Thereafter, in order to remove the oxide layer, contacting surfaces were ground using 600-grade SiC paper and then ultrasonically cleaned in an acetone bath. An interlayer was then inserted between two base metal coupons. A brazing operation was carried out in a vacuum furnace under a vacuum of approximately 10^{-5} torr. The brazing temperature was selected as 1050°C. The brazing time was varied from 10 to 40 min.

Specimens were sectioned perpendicular to the bond and then microstructural observations were made on cross sections using an optical microscope and a field emission scanning electron microscope (FESEM). For microstructural examinations, specimens were etched using 10 mL HNO_3–10 mL $C_2H_4O_2$–15 mL HCl. Semiquantitative chemical analyses of phases formed in the centerline of the bond region and adjacent to base metal were conducted using a JEOL 5900 FESEM equipped with an ultrathin window Oxford energy-dispersive X-ray spectrometer (EDS). Element distribution across the joint region was analyzed using a JEOL JXA-8900R electron probe X-ray microanalyzer equipped with line scan wavelength dispersive spectrometry (WDS).

Microhardness testing was used to determine the joint region hardness profile. The test was conducted on sample cross sections using a 10-g load on a Buehler microhardness tester. To evaluate the mechanical strength of TLP bonds, shear testing was used instead of tensile testing. Tensile testing is not strict to the bond line. Indeed, a minimal amount of the bond line is oriented on the plane experiencing the maximum resolved shear stress (i.e., plane that oriented 45 deg to the tensile axis) (Ref. 22). Therefore, it can be deduced that tensile testing of a TLP bond with a thin interlayer (i.e., 50 μm) does not effectively test the bond line. Therefore, a fixture was designed for shear testing — Fig. 1. The designed fixture subjects the sample to a pure shear stress at the bond line. Despite the fact that this testing method is not a standard one and is primarily comparative, the results are sensitive to the joint microstructure. Room-temperature shear testing was performed employing an Instron tensile machine with a cross-head speed of 2 mm/min. The edge effects were eliminated by machining before the shear test.

Results and Discussion

Typical Microstructure of Diffusion Brazed IN718

During diffusion brazing, the following metallurgical phenomena occurs:

1. Melting of filler metal
2. Dissolution of the base metal
3. Diffusion of MPD elements into the base metal
4. Solidification of liquid phase, which can occur via two different mechanisms, isothermal solidification at the brazing temperature and athermal solidification upon cooling.

When the base metal/filler metal assembly is heated to the brazing temperature, the filler metal melts. This is because the liquidus temperature of the filler metal is lower than the brazing temperature. To achieve equilibrium at the solid/liquid interface, the composition of the solid base metal is brought to the solidus at brazing temperature via dissolution of the base metal (Ref. 18). This process modifies the chemical composition of the liquid phase adjusting it to the liquidus composition at brazing temperature. Once local equilibrium is achieved,

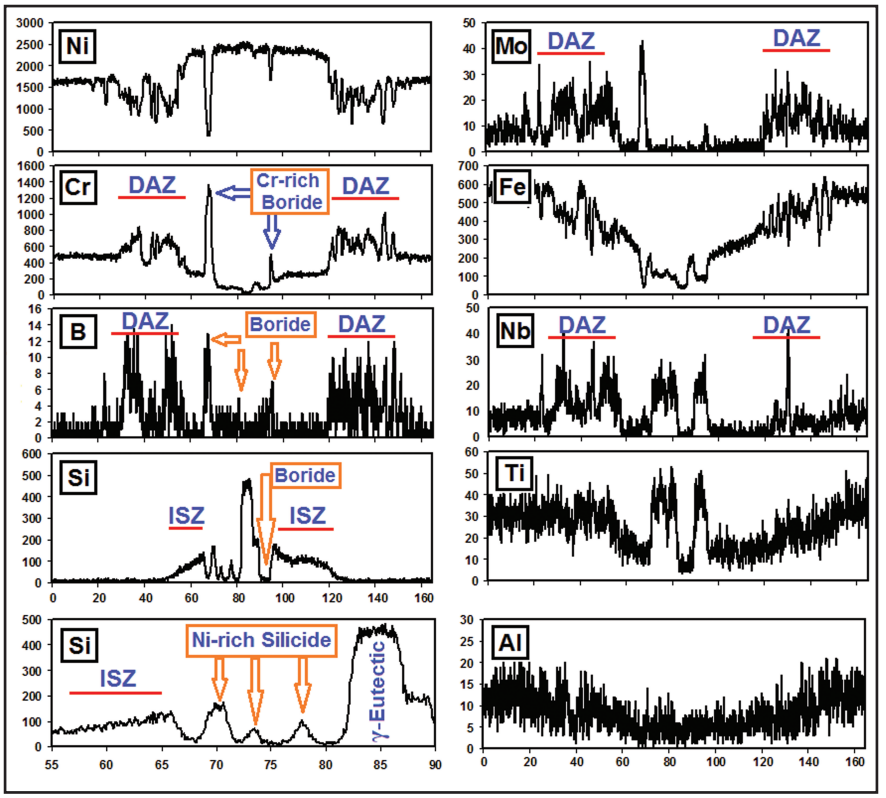

Fig. 3 — EPMA line scan across the BM, DAZ, ISZ, and ASZ in material diffusion brazed at 1050°C for 10 min.

dissolution ceases. This is followed by interdiffusion of base metal and liquid phase. The diffusion of MPD elements (e.g., B and Si) from the liquid phase into the base metal and diffusion of Cr and Fe from the base metal into the liquid phase, increases the liquidus temperature (T_L) of the liquid phase. Once the liquidus temperature reaches the brazing temperature, the liquid resolidifies during holding at brazing temperature (i.e., isothermal solidification starts). Due to the absence of solute rejection at the solid/liquid interface during isothermal solidification under equilibrium condition, the only solid phase that forms is the solid solution phase, and formation of other phases is basically prevented (Ref. 11). In situations where the brazing time is not sufficient to allow complete diffusion of MPD elements in the base metal, some amount of liquid remains at the joint centerline, which can undergo eutectic-type solidification during cooling .

The joint microstructure is significantly affected by the above-mentioned phenomena. Figure 2A shows a backscattered electron SEM image of the brazes made at 1050°C for 10 min indicating four distinct microstructural zones in the joint region, namely:

1. Isothermal solidification zone (ISZ) in which the solidification of the liquid phase occurs at the brazing temperature. The driving force for isothermal solidification is a compositional change induced by interdiffusion between substrate and interlayer during holding at the brazing temperature.

2. Athermal solidification zone (ASZ) in which the solidification of the liquid phase occurs on cooling. The presence of intermetallic phases and eutectic-type morphologies are the main feature of this region.

3. Diffusion-affected zone (DAZ) in which the microstructure is influenced by the solid-state diffusion of MPD elements into the base metal (BM). This zone is featured by secondary phase precipitates (mainly boride in the case of B-containing filler metals).

4. Base metal in which the microstructure is not affected by diffusion of MPD elements during the brazing process.

The corresponding element redistribution across the joint region is shown in Fig. 3 indicating significant chemical composition inhomogeneity across the braze region. In the following section, the microstructural evolution in each zone is described and analyzed.

Table 1 — EPMA/WDS Based Chemical Composition of Microconstituents in the ISZ and ASZ of Diffusion Brazed IN718 at 1050 for 10 Min

Element	ISZ	Ternary Eutectic	Eutectic γ	Nickel-Rich Boride	Cr Boride
Ni	73.55	64.82	75.3	62.26	8.59
Cr	10.95	4.55	6.74	4.54	29.57
Si	6.93	12.57	11.92	0.57	0.02
B	—	12.52	—	27.28	49.47
Nb	0.34	1.2	0.42	1.5	0.89
Mo	0.26	0.06	0.18	0.07	9.14
Fe	7.52	3.88	5.2	2.97	2.13
Ti	0.19	0.32	0.12	0.69	0.19
Al	0.26	0.08	0.12	0.12	—

Isothermal Solidification Zone (ISZ)

As can be seen in Fig. 2A, the microstructure of the ISZ consists of a single-phase solid solution. This zone is formed due to diffusion-induced isothermal solidification. According to the typical EDS spectrum (Fig. 4A) and typical WDS analysis (Table 1), the ISZ consists of a Ni-rich γ phase. Presence of elements such as Mo, Nb, Al, and Ti that were not present in the initial interlayer composition (Ni-7Cr-3Fe-4.5Si-3.2B) indicates dissolution of the base metal. According to EPMA line scan analysis (Fig. 5), this region contains a higher amount of Ni but smaller amounts of Cr, Fe, Nb, and Mo compared to the base metal. No B was detected in the ISZ using the WDS technique (Table 1); however, Si tends to build up in the ISZ (Fig. 3) due to its relatively low diffusion coefficient compared to B.

Athermal Solidified Zone (ASZ)

Figure 2B shows an optical micrograph of athermal solidification products. Figure 2C, D shows the SEM images indicating the details of ASZ microconstituents. Due to their specific morphologies, it can be inferred that they were formed during eutectic-type reactions. Based upon the chemical analysis of the phases, it can be inferred that the microstructure of ASZ consisted of (1) binary eutectic of Ni-rich boride (marked by M in Fig. 2C) and γ solid solution, (2) binary eutectic of Cr-rich boride (marked by N in Fig. 2C) and γ solid solution, and (3) ternary eutectic of Ni-rich boride (marked by R in Fig. 2D), Ni-rich silicide (marked by S in Fig. 1D), and γ solid solution. A typical EDS spec-

trum is shown in Fig. 4 for each intermetallic phase. The chemical compositions of the intermetallic phases and eutectic-γ were determined using EPMA and are listed in Table 1. The chemical compositions of individual phases in ternary eutectic could not be determined using EPMA due to their very fine size.

The microstructure development during athermal solidification is controlled by two interlinked phenomena: formation of γ -Ni rich dendrites and the subsequent segregation of elements (Ref. 23). During continuous formation of γ dendrites, solute elements with partitioning coefficient k < 1 are rejected into liquid. Continuous solute enrichment of liquid could cause solute concentration to exceed the solubility limit of solute in the γ phase; therefore, secondary solidification constituents are formed between dendrites (Refs. 23, 24). Therefore, to explain the solidification behavior of the residual liquid, it is necessary to study the segregation behavior of elements during solidification. Here, two parameters are used to describe the segregation tendency of the elements:

Distribution coefficient (k): The distribution coefficient (k) describes the extent and direction of microsegregation during solidification of the alloy. Values of k less than unity indicate that dendrite cores will be depleted in the particular alloying element relative to interdendritic regions, while values greater than unity imply the opposite behavior. A k value of unity implies that no dendritic microsegregation will occur. Under equilibrium conditions and by neglecting undercooling at the dendrite tips and neglecting the solid-state backdiffusion, the first solid to form from the liquid, which is the dendrite core, will have a composition of kC_0, where C_0 is the nominal composition of the alloy and k is the equilibrium partition coefficient (Ref. 24). Therefore, the ratio between dendrite core composition and the nominal composition will yield the partition coefficient at the beginning of the solidification process. Since it is difficult to determine the k values for the diffusion brazing region, they were calculated for the cast base metal. The composition of the dendrite core in cast base metal was determined using EPMA analysis. The calculated k values are reported in Fig. 5. The obtained k values are in good agreement with the published k value for IN718 in the literature (Refs. 25, 26). The B concentration profile cannot be unequivocally determined using the used analytical techniques. However, it is expected that B will segregate to the liquid phase during solidification based on the behavior of B in the Ni-B binary system where the value of k of B in hypoeutectic Ni-B binary alloy is approximately 0.008 indicating severe positive segregation behavior.

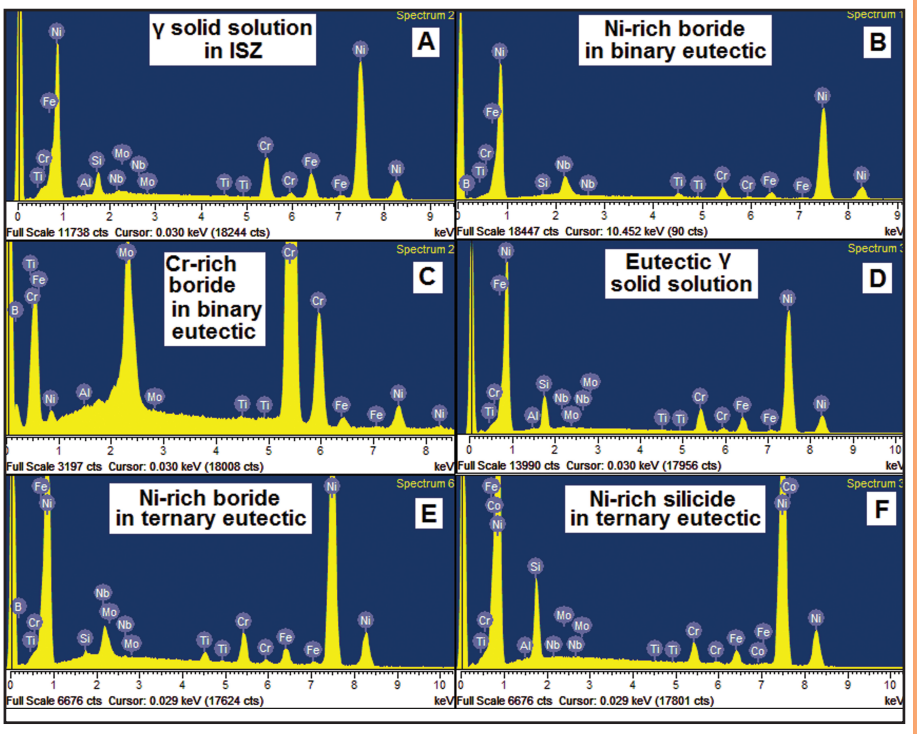

Fig. 4 — Typical EDS spectrum: A — ISZ; B — Ni-rich boride in binary eutectic; C — Cr-rich boride in binary eutectic; D — Eutectic gamma (γ) solid solution; E — Ni-rich boride in ternary eutectic; F — Ni-rich silicide in ternary eutectic in TLP bonded IN718 after partial isothermal solidification.

Partitioning coefficient (P): In addition to the distribution coefficient, a good guide to determining which element promotes stability in which phase is given by the segregation behavior of components among the phases present (Ref. 25). A partition coefficient can be defined for a partial isothermally solidified joint as the ratio of element concentration in a microconstituent in athermally solidified products to its concentration in the isothermally solidified zone. The partition coefficient were calculated for each phase except boron and are given in Table 2.

Now, considering the distribution coefficient and partition coefficient, the solidification sequence can be explained in four stages:

• Stage 1 — Formation of Ni-rich γ primary solidification phase: The solidification path begins with γ primary enriching the remaining liquid in elements with k < 1. According to Fig. 5, therefore, the liquid is enriched in B, Si, Nb, Mo, and Ti.

• Stage 2 — Formation of binary eutectic of Ni-rich boride and Ni-rich γ solid solution: The growth of γ dendrites continues until the liquid composition at the γ/liquid interface satisfies the three-phase noninvariant eutectic reaction of $L \rightarrow$ *Ni-rich Boride* + γ. According to the EPMA map (Fig. 3) and calculated partitioning coefficient (Fig. 5), the Ni-rich boride is enriched in Nb and Ti. The high value of P for Nb and Ti in Ni-rich boride indicates they promote the formation of Ni-rich boride. According to EPMA analysis, the amount of B in Ni-rich boride is about 27 at.-%, which is much higher than the initial composition of filler metal (i.e.,

Table 2 — Partition Ratio of Various Elements in Ni-Rich Boride, Cr-Rich Boride, and in Ternary Eutectic

Element	In Ni-Rich Boride	In Cr-Rich Boride	In Ternary Eutectic
Ni	0.85	0.12	0.88
Cr	0.41	2.7	0.41
Si	0.08	0.00	1.81
Nb	4.41	2.62	3.53
Mo	0.27	35.15	0.23
Fe	0.4	0.28	0.52
Ti	3.63	1	1.68
Al	0.46	0	0.31

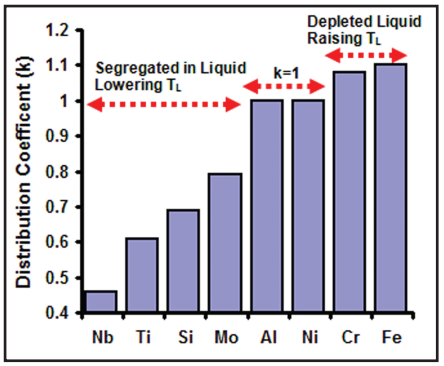

Fig. 5 — Calculated distribution coefficient of alloying elements in cast IN718.

14.4%) indicating severe segregation of B during athermal solidification. Considering the boron content in the Ni-rich boride, it can be deduced that this boride phase is the Ni_3B type.

• Stage 3 — Formation of binary eutectic of Cr-rich boride and γ solid solution: According to Table 2, formation of Ni-rich boride enriches the remaining liquid in Si, Cr, and Mo. This shifts the liquid composition toward formation of a pseudo-binary eutectic of Cr-rich boride and γ phase. According to the EPMA map and partition coefficient given in Table 2, the Cr-rich boride is highly enriched in Mo compared to the isothermally solidified zone. The B content of Cr-rich boride (i.e., 49 at.-%) is also much higher than its value in the initial composition in the filler metal indicating severe positive segregation of B during solidification. Considering the B content in the Cr-rich boride, it can be deduced that this boride phase is CrB.

• Stage 4 — Formation of ternary eutectic of Ni-boride, Ni-silicide and γ: According to the low distribution coefficient of Si and low partition coefficient of Si in Ni-rich boride and Cr-rich boride, formation of boride phases is accompanied by Si rejection into the residual liquid. Although the B content in the residual liquid is consumed largely during stage 2 and stage 3, some amount of B remains in the last portion of the liquid. The enrichment of liquid in Si and B, shifts the composition of the melt toward ternary eutectic composition and thus Ni-rich boride, Ni-rich silicide, and γ-solid solution are formed. It is interesting to note that initial Si content of the filler metal (~7.8 at.-%) is much lower than the solubility limit of Si in Ni (~ 15 at.-%); therefore, formation of silicide phase during solidification can be related to the segregation behavior of Si and rejection of Si due to the formation of boride phase. According to the EPMA line scan (Fig. 3), the boride phases are almost Si free; therefore, their formation increases the Si content in the liquid phase and subsequently promotes formation of silicide during solidification.

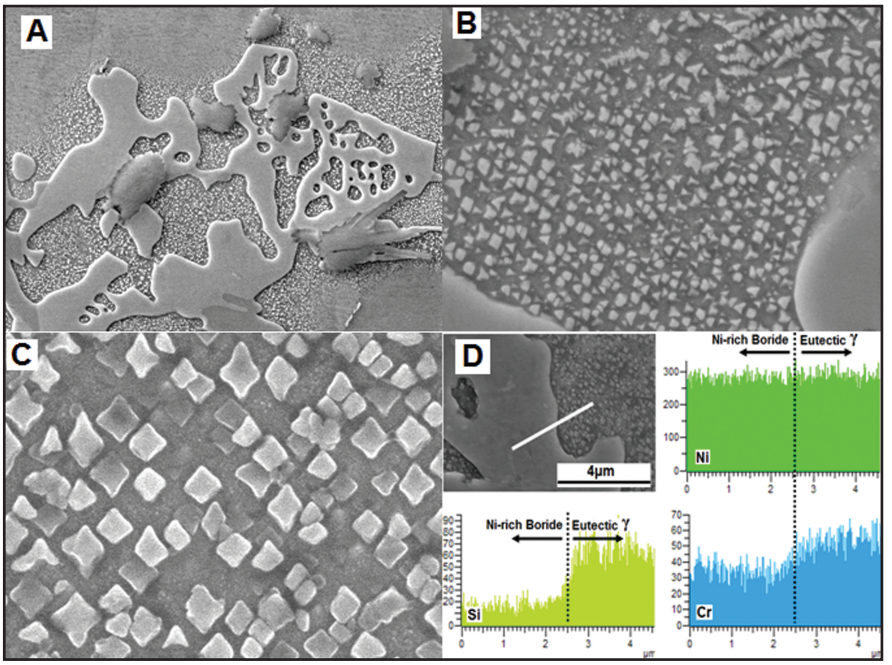

Fig. 6 — A — Formation of Ni_3Si in eutectic gamma solid solution; B, C — higher magnification view of Ni-silicide; D — X-ray elemental map across the Ni-rich boride/eutectic gamma solid solution.

Accordingly, the solidification sequence can be summarized as follows:

L → γ + L → γ + Ni-rich Boride + L → γ + Ni-rich Boride + Cr-rich Boride + L → γ + Ni-rich Boride + Cr-rich Boride + Ni-rich Silicide

It is interesting to note that eutectic-γ and proeutectic γ contain extensive fine precipitation — Fig. 6A. Figure 6B, C shows a high-magnification view of the morphology of these precipitates. Due to their small sizes (20 to 30 nm), they cannot be directly analyzed. However, WDS analysis Table 1 and EPMA map of Si in Fig. 3 showed a high concentration of Si in this region. Moreover, an EDS X-ray line scan across the eutectic-γ and its adjacent Ni-rich boride (Fig. 6D) clearly shows a high concentration of Si in this region. The high Si content of eutectic-γ is due to segregation of Si during solidification and its tendency to partition in the boride phase, as explained above. The morphology of these fine precipitates suggests they were formed during a solid-state precipitation reaction during cooling, not directly from solidification of the remaining liquid. According to the Ni-Si binary phase diagram (Ref. 28), the solubility of Si in Ni at 1050°C is about 15 at.-%, while its solubility is decreased to 8 at.-% at room temperature. Consequently, the β_1-Ni_3Si phase precipitated from Si-rich γ solid solution during cooling. Unlike the intermetallic phases formed during athermal solidification that formed interlinked networks, the isolated Ni_3Si precipitates would not be expected to have a detrimental effect on joint mechanical strength.

Diffusion-Affected Zone (DAZ)

In addition to the centerline eutectic, significant secondary phase precipitates were observed at the bond line and base metal. Figure 7 shows the interface microstructure of the joint/base metal. It is seen that microstructure of the DAZ consists of second-phase particles with both Widmanstätten (Fig. 7A) and blocky (Fig. 7B) morphologies. These precipitates appeared close to the joint interface. The size of this region is about 40 μm. Figure 8 shows the X-ray line scan across a blocky precipitate in the DAZ indicating partitioning tendencies of various elements that are present in the particle compared to that of the adjacent austenitic γ matrix. As can be seen, the precipitate is enriched with Cr, Mo, Nb, and B, while it is lean in Fe and Ni. No partitioning tendency was detected for Si and Ti. Therefore, this confirms that these secondary phases are Cr-Mo-Nb based borides. Moreover, according to the EPMA line scan (Fig. 3), the discrete peaks of B, Nb, Cr, and Mo in the DAZ correspond to the formation of boride precipitates in this region.

The morphology of these suggests that these precipitates are not formed during solidification. Formation of boride precipitates in the DAZ is directly associated with B diffusion out of liquid into the base metal during the brazing process. Consid-

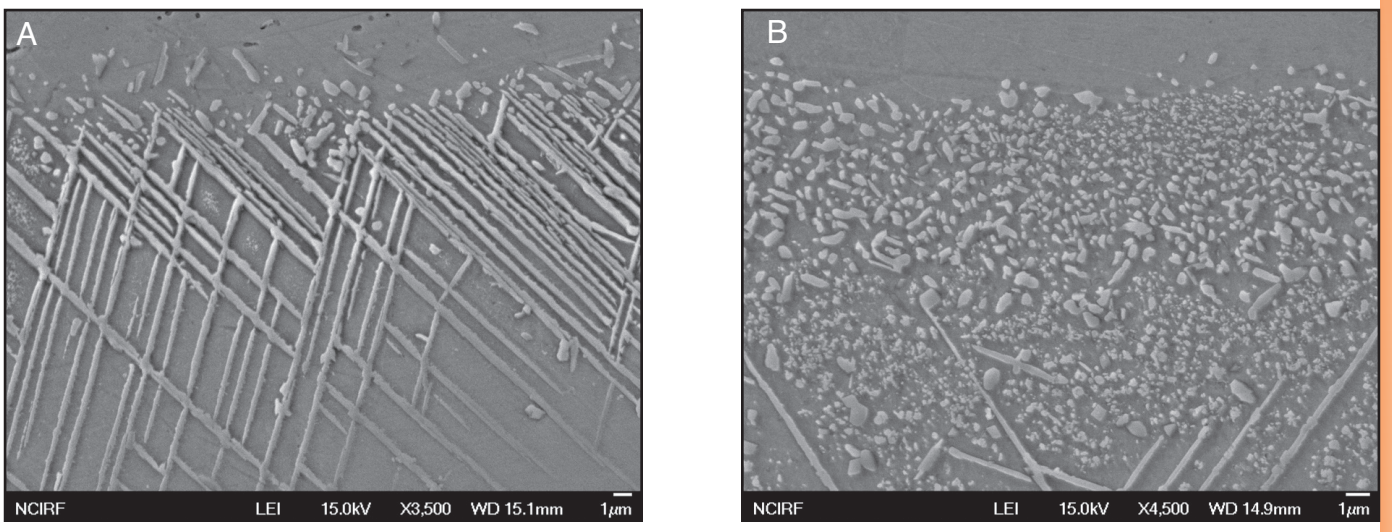

Fig. 7 — Precipitation in DAZ. A — Widmanstätten-type borides; B — blocky borides.

ering the fact the isothermal solidification is controlled by diffusion of B into the base metal, the formation of boride precipitates in the DAZ is possible. Moreover, Gale and Wallach (Ref. 29) in their work on microstructural development in transient liquid phase brazing of Ni substrate with a Ni-Si-B interlayer at 1065°C have observed formation of Ni_3B particles at the original joint/base metal interface. They suggested that contrary to the predictions of currently available diffusion brazing models, a significant solid-state diffusion of B occurs in the base metal before completion of the dissolution process such that the solubility limit of B in the base metal was exceeded at brazing temperature.

Due to diffusion of B into the base metal, a B-containing alloy is formed in a narrow region in the substrate zone adjacent to the ISZ. The solubility of B in this alloy is limited. This fact coupled with the presence of Cr, Mo, and Nb in the matrix that are strong boride formers can explain the formation of Cr-Mo-Nb-rich precipitates. Gale and Wallach (Ref. 29) provided some evidence confirming that these precipitates are formed at the brazing temperature not during cooling.

It is interesting to note that the formation of secondary precipitates in the DAZ is not associated with the diffusion of Si, as a MPD element in filler metal. This is due to the following reasons:

1. The solubility limit of Si in nickel-based alloy is higher than that of the B in nickel-based alloys. According to the Ni-Si binary phase diagram, the solubility of Si in Ni is 8 at.-%, which is much higher than the solubility of B in Ni (0.3 at.-%, according to binary Ni-B equilibrium phase diagram (Ref. 28)). This prevents the formation of silicides in the DAZ.

2. The diffusion coefficient of Si in Ni is much lower than that of B in Si. As can be seen in the EPMA profile in Fig. 2, there is no Si buildup in the DAZ. Most of the Si is concentrated in the ISZ due to its low diffusion coefficient. Accordingly, it can be concluded that the maximum solubility of Si in the substrate region cannot be exceeded and thus formation of silicide secondary phases in the DAZ is prohibited.

Formation of Cr-Mo-Nb in the DAZ leads to a significant depletion of Cr and Mo around these precipitates. This reduces the local corrosion resistance of the matrix (Cr and Mo are two key elements in corrosion behavior of IN718). Moreover, the aging behavior of IN718 strongly depends on the Nb content of the alloy (Ref. 30). Therefore, the presence of extensive Cr-Mo-Nb-based borides present in the DAZ that depletes the adjacent matrix from Nb can affect the aging behavior of this region (Refs. 31, 32).

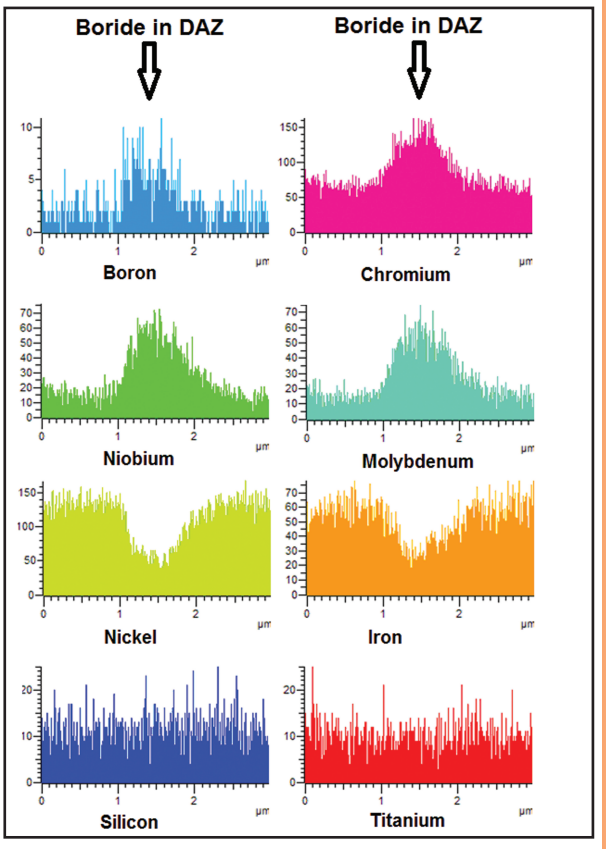

Fig. 8 — X-ray line scan across blocky secondary precipitates in the DAZ.

Effect of Brazing Time on Bond Microstructure and Hardness Characteristics

Joint microstructure that significantly affects the joint performance depends on elemental interdiffusion between base metal and interlayer, which in turn is governed by brazing time. The average width of the isothermally solidified zone is measured at each brazing time and its variation with respect to square root of brazing time is plotted in Fig. 9A. As can be seen, there is a linear relation between ISZ size and root of brazing time. The implication is that the formation of gamma solid solution is a diffusion-controlled process. Indeed, in the case of diffusion brazing of IN718/Ni-Cr-Fe-Si-B/IN718, the isothermal solidification process is controlled by formation and growth of γ-solid solution, which is governed by MPD element diffu-

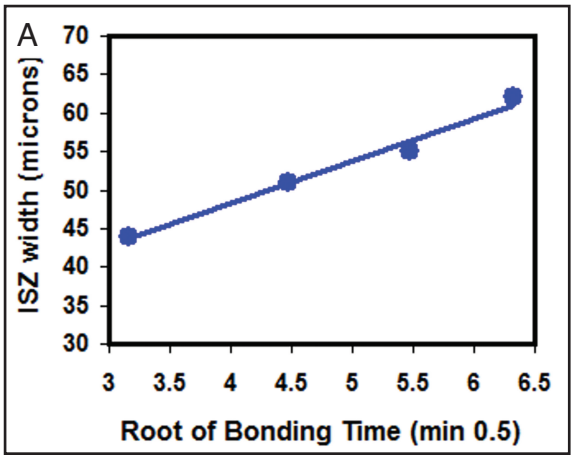

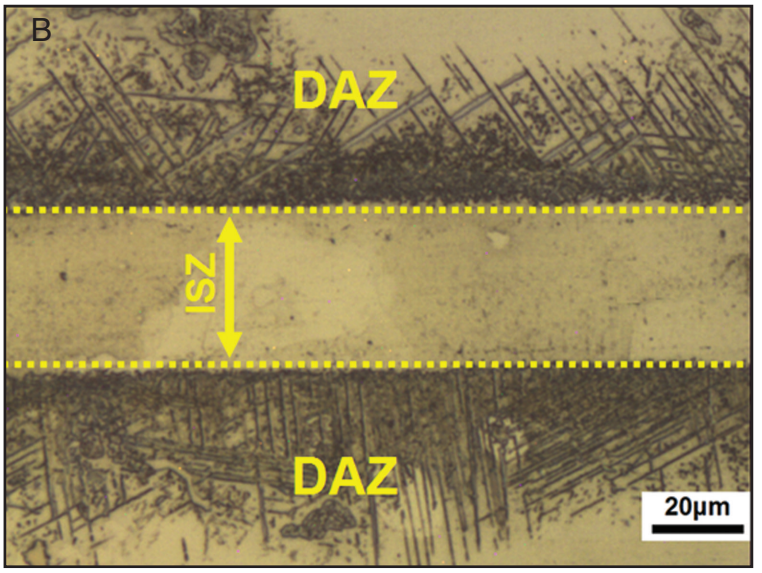

Fig. 9 — A — Variation of width of isothermally solidified gamma solid solution with root of bonding time; B — microstructure of isothermally solidified diffusion brazed IN718 at 1050°C for 40 min showing a eutectic-free joint centerline.

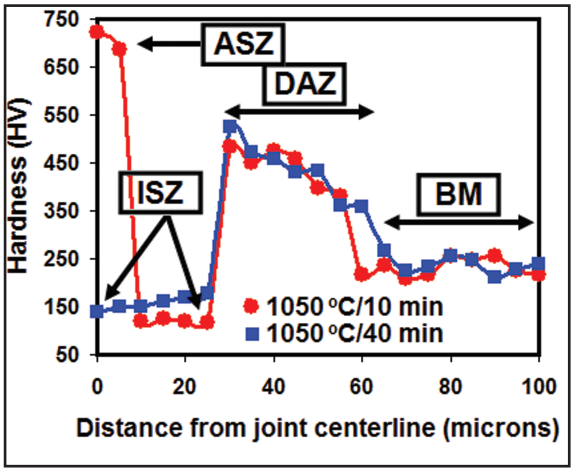

Fig. 10 — Hardness distribution across the bond region for diffusion brazed IN718 at 1050°C for 10 min with partial isothermal solidification and 1050°C for 40 min with complete isothermal solidification.

sion in the base metal. Increasing brazing time reduces the volume fraction of eutectic-type microconstituent in the joint centerline. When brazing time increased to 40 min, no eutectic structure was observed in the bond region — Fig. 9B. Therefore, it is concluded that a holding time of 40 min at 1050°C is sufficient for isothermal solidification completion.

Figure 10 shows the hardness distribution across the braze region for brazes made at 1050°C for 10 min. The hardness distribution across the joint can be well correlated to the microstructural gradient across the braze region. The average base metal hardness is 230 HV, which corresponds to the γ matrix of cast IN718. The average hardness of the ASZ is about 700 HV, which is related to the formation of intermetallic-containing eutectic-type solidification products. The hardness of ISZ averaged 120 HV, which is lower than the base metal. According to the EPMA line scan (Fig. 3), the ISZ exhibits a lack of sufficient Nb, Al, Ti, Cr, and Mo compared to the base metal, which explains its lower hardness. The average hardness of the DAZ is 440 HV. The higher hardness of the DAZ compared to the base metal is directly associated to the formation of Cr-Mo-Nb rich boride phase in the γ matrix.

The effect of isothermal solidification on the hardness profile is also superimposed in Fig. 10. Since the isothermal solidification eliminates the eutectic-type microconstituent, it is not surprising that the peak hardness in the joint centerline is not present. The hardness of ISZ after completion of isothermal solidification is increased compared to ISZ of joints made at 1050°C for 10 min. This can be related to more diffusion of alloying elements (e.g., Nb, Cr, Mo, Al, and Ti) from base metal into the bond region with increasing brazing time enhancing the solid solution strengthening contribution. However, completion of isothermal solidification does not influence the peak hardness in DAZ. This is due to the fact that boride precipitates in DAZ are still stable even after isothermal solidification completion.

Shear Strength

The mechanical properties of the diffusion brazed joint are described in terms of maximum shear strength, total strain at failure point (fracture strain), and fracture energy (defined as the area under stress-strain curve up to failure point). The joint strength and fracture of diffusion brazed joints depend on the bond microstructure. Since the microstructure development is significantly affected by brazing time (Fig. 9A), it is expected that the brazing time may have a significant effect on the mechanical properties of the joints. Effect of brazing time on the shear strength, failure elongation, and failure energy of joined cast IN718 is shown in Fig. 11. As can be seen, the shear strength, failure elongation, and failure energy of joints made at 1050°C for 10 min are the lowest. Metallographic examination of the cross section of the fractured sample (Fig. 12A, B) showed the failure occurred via crack propagation through the ASZ. High hardness of eutectic products (Fig. 10) coupled with the fact that nickel boride phase forms an interlinked network, provide a metallurgical notch that significantly decreases the load-carrying capacity of the joint. The low ductility of the intermetallic leads to low fracture strain and fracture energy of partially isothermally solidified joints. Scanning electron micrograph fractorgraphy of the fracture surface along with an X-ray map are shown in Fig. 12C–E. As can be seen, the fracture surface exhibits a semi-cleavage morphology that confirms the low failure energy of this joint. The X-ray map of the fracture surface (Fig. 12E) also indicates crack propagation through athermal solidification products. Based upon the X-ray elemental map (Fig. 12E) and SEM-EDS chemical analysis (not shown here), it can be inferred that the locations marked as X, Y, and Z (Fig. 12D) are Cr-rich boride, eutectic-γ and Ni-rich boride precipitates. As can be seen, the interlinked network of Ni-rich boride is the main source for the fracture of the joint. Therefore, it is necessary to eliminate the eutectic products in order to improve joint strength.

According to Fig. 11, increasing brazing time improves the mechanical properties of the joints in terms of shear strength, fracture strain, and fracture energy. This can be related to the decrease in the width

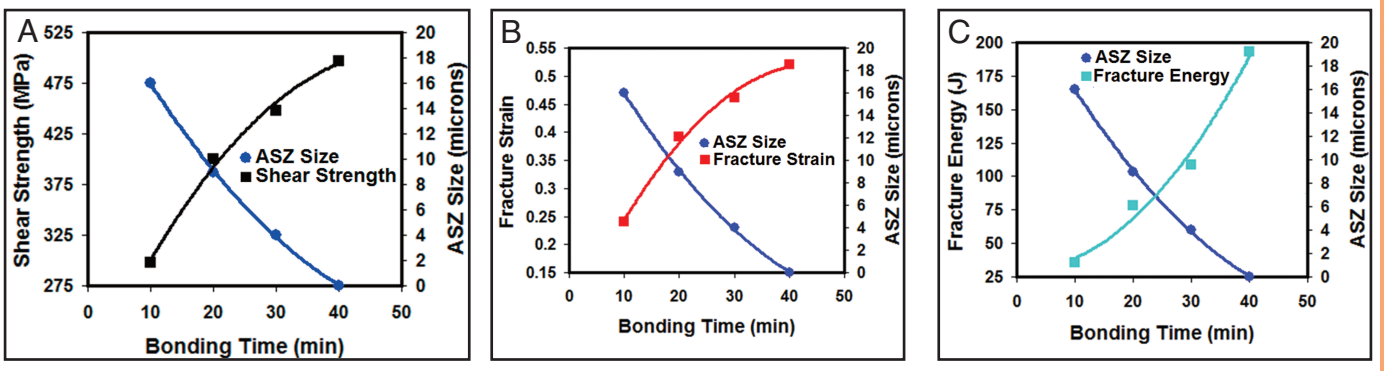

Fig. 11 — Effect of joining time and width of eutectic-type microconstituents (ASZ size) on the mechanical properties of diffusion brazed IN718: A — Shear strength; B — fracture strain; C — fracture energy.

of the eutectic-type microconstituents. According to Fig. 11A–C, there is an inverse relation between width of the ASZ and mechanical properties of the joint. Therefore, it can be deduced that in a brazing condition in which isothermal solidification is not completed, the extent of the eutectic constituent (ASZ) is the controlling factor for the shear strength, fracture strain, and fracture energy.

When brazing time increased to 40 min at 1050°C, a joint with a shear strength of about 497 MPa was achieved. This can be related to the complete removal of the eutectic-type microconstituents in the joint centerline producing a single-phase solid-solution microstructure across the joint region. The shear strength of base metal heat treated at 1050°C for 40 min is about 660 MPa. Therefore, a joint efficiency of 75% was obtained after completion of isothermal solidification. The lower shear strength of the joint in this condition compared to the base metal is related to the soft ISZ relative to the base metal. Higher joint efficiency can be achieved via designing a proper postbraze heat treatment to improve the homogenization across the braze region via enhancing the interdiffusion of alloying elements, particularly Nb, Cr, and Mo, and eliminating the boride precipitates in the DAZ.

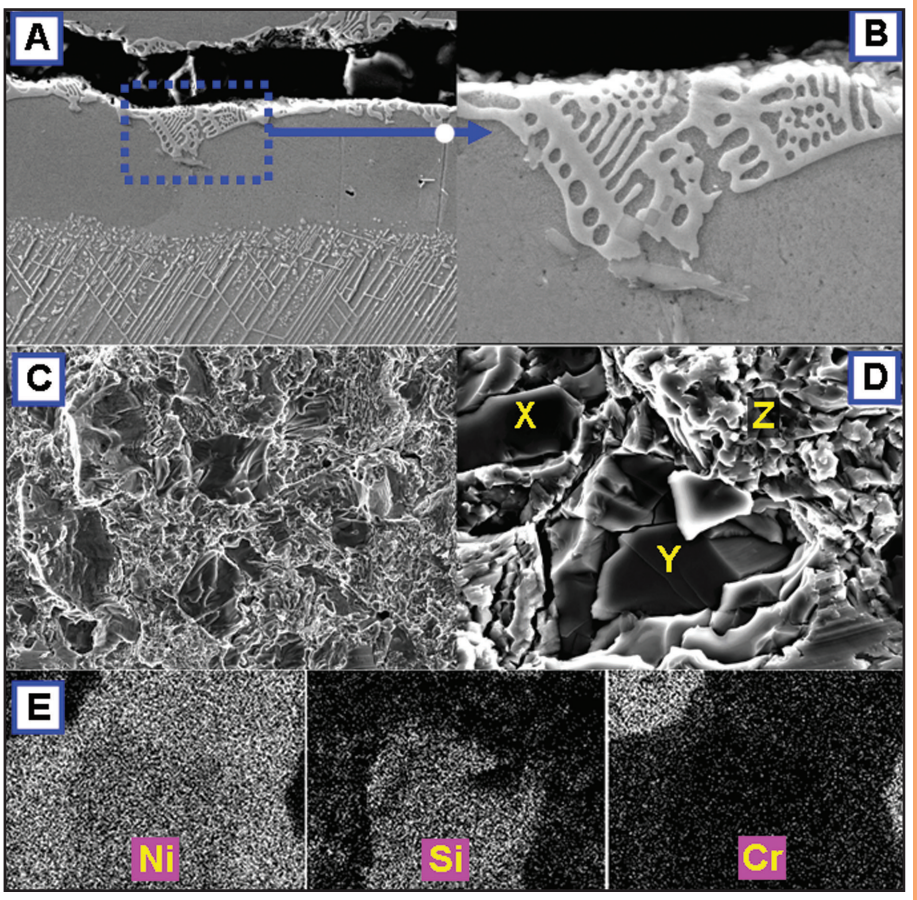

Fig. 12 — A — Fracture path during shear testing of cast IN718 diffusion brazed at 1050°C for 10 min; B — magnified view of fracture location in A; C — morphology of fracture surface; D — higher magnification view of fracture morphology; E — X-ray map of Ni, Si, and Cr from selected location (D) of fracture surface. The locations marked as X, Y, and Z are Cr-rich boride, eutectic-γ and Ni-rich boride.

Conclusions

For this study, microstructure development and mechanical properties of diffusion brazed IN718 nickel-based superalloy were investigated. The following conclusions can be drawn from this study:

1) The joint microstructure is influenced by complicated phase transformations including diffusion-induced isothermal solidification, cooling-induced athermal solidification, and difusion-induced solid-state precipitation. After partial isothermal solidification, three distinct microstructural zones were formed in the brazing-affected zone: isothermal solidification zone (ISZ), which consisted of Ni-rich γ solid solution; athermal solidification zone (ASZ), which consisted of eutectic-type microconstituents; and diffusion-affected zone (DAZ), which consisted of extensive boride precipitates distributed in the matrix.

2) When the brazing time is not sufficient to complete solidification of the liquid phase at the brazing temperature, the residual liquid is solidified on cooling. The solidification behavior of residual liquid is governed by low solubility of Si and B and their segregation behavior. Solidification of the residual liquid is started by solidification of Ni-rich γ dendrites enriching the remaining melt with B and Si. This follows by formation of binary eutectic of γ-Ni-rich and Ni-rich boride and then by formation of binary eutectic of γ-Ni-rich and Cr-rich boride. The formation of boride phases enriches the remaining melt in Si leading to formation of ternary eutectic of Ni-Si-B as the last solidified portion.

3) Extensive fine Ni-rich silicide (γ′-Ni_3Si) formed within the eutectic γ by

solid-state precipitation due to the decreased solubility of Si in nickel at lower temperatures. Unlike the intermetallic phases formed during athermal solidification, which formed interlinked networks, the isolated Ni_3Si precipitates would not be expected to have a detrimental effect on joint mechanical strength.

4) Extensive Cr-Mo-Nb-rich boride precipitates were formed in the substrate region due to boron diffusion into the base metal during the brazing process. The formation of these precipitates in the DAZ can affect the local corrosion behavior and aging response of the alloy.

5) Mechanical strength of the joint depends on the microstructure development in the joint region, which in turn is controlled by brazing time. In situations where the brazing time is insufficient to achieve complete isothermal solidification, the fracture occurs via crack propagation through the hard and brittle eutectic-type microconstituents in the joint centerline. An inverse relation between width of the ASZ and mechanical properties in terms of shear strength, fracture strain, and fracture energy is established. Completion of isothermal solidification, which resulted in a eutectic-free joint centerline improved the mechanical properties of the bonds.

Acknowledgment

One of the authors, M. Pouranvari, gratefully acknowledges the support from Prof. H. N. Han during his sabbatical leave in Department of Materials Science & Engineering, Seoul National University.

References

1. Rivaux, B., Cao, X., Jahazi, M., Cuddy, J., and Birur, A. 2009. Effect of pre- and post-weld heat treatment on metallurgical and tensile properties of Inconel 718 alloy butt joints welded using 4 kW Nd:YAG laser. *J Mater Sci* 44: 4557–4571.

2. Yeh, A. C., Lu, K. W., Kuo, C. M., Bor, H. Y., and Wei, C. N. 2011. Effect of serrated grain boundaries on the creep property of Inconel 718 superalloy. *Mater. Sci. Eng. A* 530: 525–529.

3. Pouranvari, M., Ekrami, A., and Ekrami, A. H. 2008. Microstructure development during transient liquid phase bonding of GTD-111 nickel-based superalloy. *J Alloys Comp* 461: 641–647.

4. Matthij, J. H. G. 1985. Role of brazing in repair of superalloy components — Advantages and limitations. *Mater. Sci. Technol.* 1: 608–612.

5. Rabinkin, A. 2004. Brazing with (NiCo Cr)-B-Si amorphous brazing filler metals: Alloys, processing, joint structure, properties, applications. *Sci. Technol. Weld. Joining* 9: 181–199.

6. Tung, S. K., Lim, L. C., and Lai, M. O. 1996. Solidification phenomena in nickel base brazes containing boron and silicon. *Scripta Mater.* 34: 125–133.

7. Philips, N. R., Levi, C. G., and Evans A. G. 2008. Mechanisms of microstructure evolution in an austenitic stainless steel bond generated using a quaternary braze alloy. *Metall Mater Trans A* 39(1): 142–9.

8. Sakamoto, A., Fujiwara, C., Hattori, T., and Sakai, S. 1989. Optimizing processing variables in high-temperature brazing with nickel-based filler metals. *Welding Journal* 68(3): 63–71.

9. Arafin, M. A., Medraj, M., Turner, D. P., and Bocher, P. 2007. Transient liquid phase bonding of Inconel 718 and Inconel 625 with BNi-2: Modeling and experimental investigations. *Mater. Sci. Eng. A* 447: 125–133.

10. Pouranvari, M., Ekrami, A., and Kokabi, A. H. 2008. Microstructure-properties relationship of TLP-bonded GTD-111 nickel-base superalloy. *Mater Sci Eng A* 490: 229–234.

11. Ojo, O. A., Richards, N. L., and Charturvedi, M. C. 2004. Effect of gap size and process parameters on diffusion brazing of Inconel 738. *Sci. Technol. Weld. Joining* 9: 209–220.

12. Duvall, D. S., Owczarski, W. A., and Paulonis, D. F. 1974. TLP Bonding: A new method for joining heat resistant alloys. *Welding Journal* 53(4): 203–214.

13. Thambury, R., Wallace, W., and Goldak, J. A. 1983. Post weld heat treatment cracking in superalloys. *Int. Met. Rev.* 28: 1–22.

14. Richards, N. L., Huang X., and Chaturvedi, M. C. 1992. Heat affected zone cracking in cast Inconel 718. *Mater Charact* 28: 179–87.

15. Radhakrishna, C. H., and Rao, K. P. 1997. The formation and control of Laves phase in superalloy 718 welds. *J Mater. Sci.* 32 (8): 1977–1984.

16. Ram, G. D. J., Reddy, A. V., Rao, K. P., and Reddy, G. M. 2004. Control of Laves phase in Inconel 718 GTA welds with current pulsing. *Sci. Technol.Weld. Joining* 9: 390–398.

17. Pouranvari, M., Ekrami, A., and Kokabi, A. H. 2009. Effect of bonding temperature on microstructure development during TLP bonding of a nickel base superalloy. *J Alloys Comp* 469: 270–275.

18. Gale, W. F., and Butts, D. A. 2004. Transient liquid phase bonding. *Sci. Technol. Weld. Joining* 9: 283–300.

19. Idowu, O. A., Ojo, O. A., and Chaturvedi, M. C. 2006. Microstructural study of transient liquid phase bonded cast Inconel 738LC superalloy. *Metall. Matter. Trans A* 37: 2787–96.

20. Idowu, O. A., Richards, N. L., and Chaturvedi, M. C. 2005. Effect of bonding temperature on isothermal solidification rate during transient liquid phase bonding of Inconel 738LC superalloy. *Mater. Sci. Eng. A* 397: 98–112.

21. Pouranvari, M., Ekrami, A., and Kokabi A. H. 2008. Microstructure-properties relationship of TLP-bonded GTD-111 nickel-base superalloy. *Materials Science and Engineering A* 490: 229–234.

22. Butts, D. A. 2005. Transient liquid phase bonding of a third generation gamma-titanimum aluminium alloy-Gamma Met PX. PhD thesis. Auburn University, Auburn, Ala.

23. Cieslak, M. J., Stephens, J. J., and Carr, M. J. 1988. A study of the weldability and weld related microstructure of Cabot Alloy 214. *Metall. Matter. Trans A* 19A: 657–667.

24. Ojo, O. A., Richards, N. L., and Chaturvedi, M. C. 2004. Microstructural study of weld fusion zone of TIG welded IN 738LC nickel-based superalloy. *Scripta Mater* 51: 683–688.

25. Cieslak, M. J., Headley, T. J., Knorovsky, G. A., Romig, A. D., and Kollie, T. 1990. A comparison of the solidification behavior of Incoloy 909 and Inconel 718. *Metall Mater Trans A* 21: 479–88.

26. Knorovsky, G. A., Cieslak, M. J., Headley, T. J., Roming, A. D. Jr., and Hammetter, W. E. 1989. Inconel 718 A solidification diagram. *Metall Mater Trans A* 20: 2149–2158.

27. Nakao, Y., and Shinozaki, K. 1990. *Proceedings of International Conference on High Temperature Materials*, Belgium, p. 24.

28. Massalski, T. B. (ed.). 1986. Binary alloy phase diagrams. Metals Park, Ohio: ASM International.

29. Gale, W. F., and Wallach, E. R. 1991. Microstructural development in transient liquid-phase bonding. *Metall. Trans. A* 22: 2451–2457.

30. Alam, T., Chaturvedi, M., Ringer, S. P., and Cairney, J. M. 2010. Precipitation and clustering in the early stages of ageing in Inconel 718. *Mater Sci Eng A* 527: 7770–7774.

31. Pouranvari, M., Ekrami, A., and Kokabi, A. H. 2013. Solidification and solid state phenomena during TLP bonding of IN718 using ternary Ni-Si-B filler alloy. *Journal of Alloys and Compounds* 563: 143–149.

32. Pouranvari, M., Ekrami, A., and Kokabi, A. H. 2013. Phase transformation during diffusion brazing of IN718/Ni-Cr-B/IN718. *Materials Science and Technology* 29: 980–984.

33. Pouranvari, M., Ekrami, A., and Kokabi, A. H. 2013. Transient liquid phase bonding of wrought IN718 nickel based superalloy using standard heat treatment cycles: Microstructure and mechanical properties. *Materials and Design* 50: 694–701.